

Experimental Photodynamic Therapy: 15 Years of Development

R. I. Yakubovskaya^a, N. B. Morozova^a, A. A. Pankratov^a, N. I. Kazachkina^a,
A. D. Plyutinskaya^a, T. A. Karmakova^a, T. N. Andreeva^a, Yu. B. Venediktova^a,
E. A. Plotnikova^a, E. R. Nemtsova^a, V. V. Sokolov^a, E. V. Filonenko^a, V. I. Chissov^a,
B. Ya. Kogan^b, A. V. Butenin^b, A. V. Feofanov^{c,d}, and M. G. Strakhovskaya^d

^a Herzen Moscow Research Oncological Institute,
2-i Botkinskii proezd 3, Moscow, 125284 Russia

^b Research Institute of Organic Intermediates and Dyes, State Scientific Center, Federal State Unitary Enterprise,
Bol'shaya Sadovaya ul. 1, str. 4, Moscow, 123995 Russia

^c Shemyakin and Ovchinnikov Institute of Bioorganic Chemistry, Russian Academy of Sciences,
ul. Miklukho-Maklaya 16/10, Moscow, 117871 Russia

^d Lomonosov Moscow State University, Moscow, 119991 Russia
e-mail: raisayakub@yandex.ru

Received February 1, 2013

Abstract—Photodynamic therapy and fluorescence diagnosis of malignant tumors have been actively developed over the last 15 years by the scientists participating in the Moscow Government-funded “Fight against Cancer” program. New effective photosensitizers absorbing in the long-wave spectral region were revealed. Unique agents Alasens-lio, Alasens-gel, Hexasens-lio, Phthalosens-lio, Holosens-lio, and Holosens-gel were produced and preclinically studied both *in vitro* and *in vivo*. New methods using low-intensity and pulse modes of irradiation and also combined methods of treatment by photodynamic therapy and well-known chemotherapy or laser hyperthermia were developed. Methodological recommendations for experimental studies of agents with photoinduced antitumor properties were published.

DOI: 10.1134/S1070363215010405

INTRODUCTION

Today, new treatment methods based on advances in photochemistry, photobiology, and quantum physics are increasingly used in medicine. Among these methods, photodynamic therapy is particularly successful in oncological practice. Photodynamic therapy is based on destruction of the tumor focus by reactive free radical particles arising from interaction of a photosensitizer accumulated in the tumor with the laser light whose wavelength corresponds to the absorption maximum of the photosensitizer.

Clinical trials of the photodynamic therapy and fluorescence diagnosis methods as applied to malignant neoplasms owe their success largely to the active development of appropriate experimental methods. Over 15 years, in the framework of the

Moscow Government-funded program of development and implementation of methods and means of fighting cancer and other dangerous diseases, these methods have been developed along the following lines:

- devising methodological approaches to adequately evaluating the efficacy of photosensitizers;
- *in vitro* and *in vivo* screening of different classes of photosensitizers;
- in-depth study of new photosensitizers, promising for clinical application;
- development of new agents for fluorescence diagnosis and photodynamic therapy of malignant neoplasms and antimicrobial photodynamic therapy and their pre-clinical trials, including pharmacokinetics, pharmacodynamics, and safety aspects;

- study of the mechanism of action of new agents;
- designing diagnostic and therapeutic equipment;
- development of new techniques and algorithms of photodynamic therapy in different modes (pulse, “low-intensity,” antimicrobial) and its combined use with well-known therapies (chemotherapy, laser hyperthermia).

Here, we report the main results of the 15-year activities in the field of experimental photodynamic therapy.

Abbreviations used:

B16	B16 melanoma
Colo26 (C26)	Murine colon adenocarcinoma
HEp2	Human laryngopharyngeal epidermoid carcinoma
HT29	Human colon carcinoma
LLC	Lewis lung carcinoma
PC1	Alveolar mucous liver cancer
P388	Lymphocytic leukemia
Raji	Burkitt's lymphoma
S37	S37 sarcoma
T24	Human bladder carcinoma

Devising Methodological Approaches to Evaluation of the Photoinduced Antitumor Activity of New Photosensitizers

There exist numerous algorithms for evaluating the efficacy of photosensitizers, but the lack of appropriate methodological framework in the initial stage of their preclinical trials prevented intercomparison of the research results for the agents and selection of the most promising candidates for photodynamic therapy. Based on the results of studies of photosensitizers from different classes, we developed methodological approaches to *in vitro* and *in vivo* assessing the photoinduced antitumor activity of photosensitizers.

The efficacy of photodynamic therapy is determined by numerous factors, among which the most important are the activity of the photosensitizer, the features of its accumulation in the tumor lesion and in the surrounding tissue, the oxygen content in the irradiated area, the treatment conditions, and the irradiation regimes. The photoactivity of a dye, in turn,

is determined by its chemical structure responsible for the ability of its molecule to absorb light and undergo a transition to the activated triplet state, inducing the generation of singlet oxygen which inflicts photochemical damage to the tumor cells and tissues.

Photodynamic therapy results not only in direct damage to tumor cells but also in disease of blood vessels and connective tissue elements feeding the tumor. A less significant, but substantial contribution to the efficacy of the method may come from the immune system-mediated cytotoxic processes initiated by photodynamic therapy.

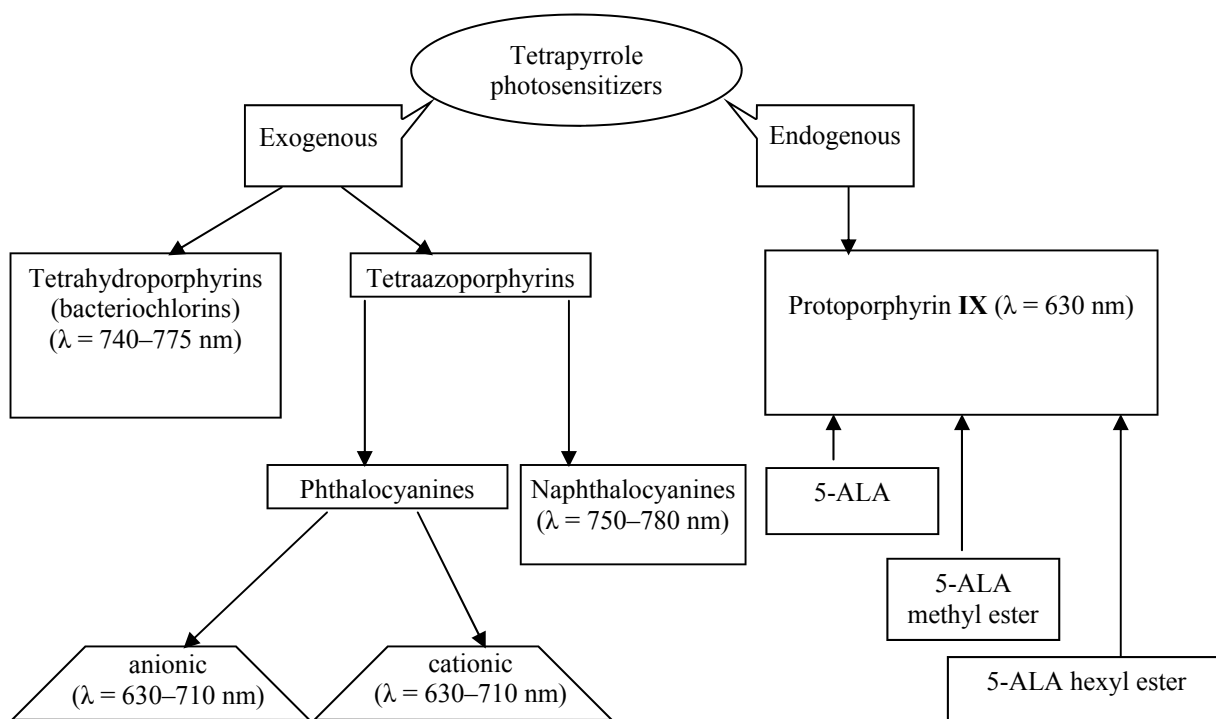
For testing new compounds with sensitizing properties we developed a multilevel evaluation system including several stages [1]: study of the physicochemical and photophysical properties of dyes, *in vitro* and *in vivo* screening of the photoinduced anti-tumor activity, and in-depth study of photosensitizers on animal transplantable tumor models.

The first stage involves assessment of the physicochemical and photophysical properties, specifically, the solubility of hydrophilic, amphiphilic, and hydrophobic compounds and their stability in the dark and under irradiation conditions, in order to identify photosensitizers soluble in biocompatible media and stable over time.

In the second (screening) stage the photoinduced cytotoxicity of compounds on a panel of mammalian tumor cells is assessed in relation to the photosensitizer concentration in the incubation medium, the time interval between the photosensitizer injection and radiation exposure, the presence/absence (removal immediately before irradiation) of dyes during irradiation.

The most efficacious photosensitizers are selected for further *in vivo* studies [2].

The third stage includes estimation of the time of maximal accumulation of the photosensitizer in tumor and of that in the period of the maximal fluorescence contrast relative to the surrounding tissue. This allows the interval between the dye administration and radiation exposure to be adequately chosen subsequently. The normalized fluorescence in animal tissues typically reflects the content of the monomeric form of the photosensitizer, which in the presence of oxygen is capable of initiating a photochemical reaction leading to the death of the tumor. The distribution dynamics of the monomeric (fluorescent) form of the photosensitizer in tissues is assessed. The efficacy of



Scheme 1. Classes of photosensitizers tested.

photodynamic therapy is estimated in relation to the photosensitizer dose, the interval between the photosensitizer administration and radiation exposure, and the radiation energy density using one of the tumor models (LLC carcinoma or S37 sarcoma). These data were used for optimizing the photodynamic treatment regimes.

In the fourth stage, an in-depth study of the photoinduced antitumor activity of the photosensitizer on animals with tumors of different genes under optimal photodynamic therapy conditions is carried out, as well as a pharmacokinetic study.

Screening of New Photosensitizers Useful for Fluorescence Diagnosis and Photodynamic Therapy

Based on the methodical approaches developed, we selected compounds with good solubility and stability in the dark and under irradiation conditions, showing no dark cytotoxicity, and characterized by high *in vitro* photoinduced tumor activity against mammalian tumor cells and high *in vivo* antitumor efficacy.

Over the last 15 years we have carried out *in vitro* and *in vivo* tests on more than 70 new endogenous and exogenous photosensitizers from different classes: synthetic tetrahydroporphyrins, phthalocyanines, and

5-aminolevulinic acid (5-ALA) esters as precursors to protoporphyrin IX (PPIX) (Scheme 1).

Tetraazaporphyrins

Tetraazaporphyrins are porphyrin series compounds having nitrogen atoms in the meso positions instead of carbon. The most studied tetraazaporphyrins are phthalocyanines and naphthalocyanines structurally close to them.

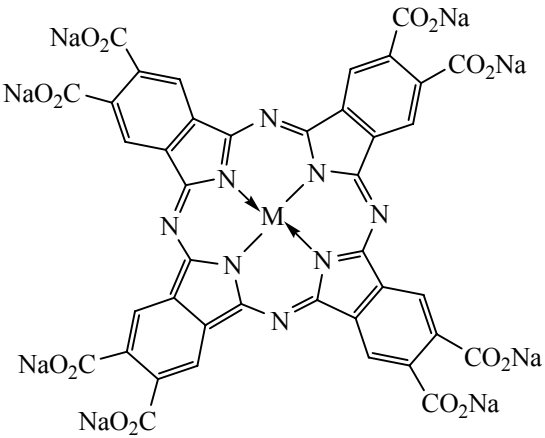
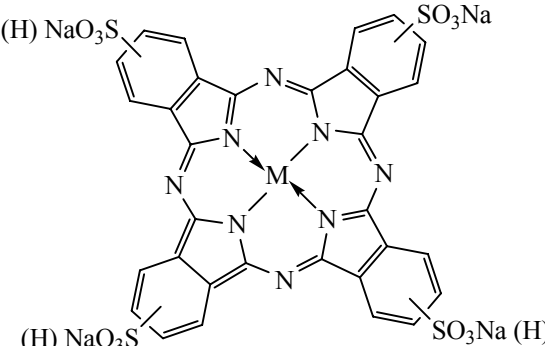
Phthalocyanines are dyes exhibiting a strong absorption band in the red and near-infrared spectral regions (670–700 nm) with a molar absorption coefficient of $1 \times 10^5 \text{ L mol}^{-1} \text{ cm}^{-1}$. The quantum yield of singlet oxygen for these compounds is 0.3–0.6.

In this study, we examined negatively and positively charged phthalocyanine derivatives.

Among negatively charged phthalocyanine derivatives, we tested phthalocyanines with lateral substituents of different nature (with sulfonic and carboxy groups), different central metal atoms (Al, Zn, Mg), and different degrees of sulfonation (see Table 1).

Studies of the absorption and fluorescence properties of the phthalocyanine derivatives showed that the metal-containing compounds in biological fluids occur in a partially aggregated, and metal-free compounds, in the completely aggregated form.

Table 1. Negatively charged phthalocyanine derivatives

Comp. no.	Macrocycle	Central atom M	Designation
I		Zn	ZnPc(COONa) ₈
II		Al	AlPc(COONa) ₈
III		HH	H ₂ Pc(SO ₃ Na) _{1.5}
IV		HH	H ₂ Pc(SO ₃ Na) _{2.5}
V		Mg	MgPc(SO ₃ Na) _{2.5}
VI		Zn	ZnPc(SO ₃ Na) _{2.5}
VII		HH	H ₂ Pc(SO ₃ Na) ₃
VIII		Mg	MgPc(SO ₃ Na) ₃
IX		Zn	ZnPc(SO ₃ Na) ₃
X		HH	H ₂ Pc(SO ₃ Na) _{3.8}
XI		Mg	MgPc(SO ₃ Na) _{3.8}
XII		Zn	ZnPc(SO ₃ Na) _{3.8}

Introduction of Cremophor EL and Triton X-100 surfactants into a biological medium results in monomerization of the photosensitizers. Aluminum and zinc carboxyphthalocyanine derivatives exhibit lower stability over time, whereas all the sulfonated phthalocyanine derivatives showed stability in the time interval selected (24 h).

The biological *in vitro* tests showed that the photosensitizers do not possess dark cytotoxicity against tumor cells (when used at 0.05–2 μM concentrations). The photoactivity of aluminum and zinc octacarboxyphthalocyanine towards HEP2 cells is significantly lower than that of the sulfonated derivatives [AlPc(COONa)₈ and ZnPc(COONa)₈ have IC_{50}^1 of 200 ± 1.5 and 160 ± 2.1 μM , respectively].

¹ The inhibitory concentration causing cell death by 50%.

Among the sulfonated derivatives, the most active are the zinc and magnesium compounds, as well as the metal-free compound with predominant content of di- and trisulfonic acid groups (IC_{50} 0.2 ± 0.1 μM , on the average) (Fig. 1) [3]. The sensitivity of the cells to photodynamic effects increases as HT29 < T24 < A549 < HEP2 < Raji (IC_{50} 3.2 ± 0.08 , 1.8 ± 0.1 , 0.52 ± 0.11 , 0.25 ± 0.08 , and 0.04 ± 0.07 μM , respectively).

The metal-free sulfonated derivative H₂Pc(SO₃Na)_{2.5} was selected for further animal experiments and was used for development of Phthalosens-liv agent whose preclinical testing has been completed to date.

Positively charged phthalocyanine derivatives are considered as suitable candidates not only for photodynamic therapy of cancer but also for antimicrobial photodynamic therapy. We tested cationic phthalocyanine derivatives with different central metal atoms

and different charge-carrying substituents (Table 2). The absorption and fluorescence analysis showed that the compounds are stable in solutions over time; the metal-free choline phthalocyanine derivative $\text{H}_2\text{PcChol}_8$ that demonstrated the lowest stability in Eagle's medium supplemented with 7% fetal bovine serum was not used in further experiments.

The cationic phthalocyanine derivatives have no dark toxicity towards tumor cells. In the series of choline and pyridinium derivatives, the highest photoinduced activity is exhibited by zinc complexes ZnPcChol_8 and ZnPcPy_8 with IC_{50} of 0.3 ± 0.08 and $0.35 \pm 0.1 \mu\text{M}$, respectively. All the compounds tested are able of penetration into and accumulation in the tumor cells. A comparative study of the photodynamic effect exerted by choline zinc phthalocyanine derivative on human tumor cells of different genes showed that the most sensitive are HEP2 cells ($0.30 \pm 0.08 \mu\text{M}$), and the least sensitive, HT29 cells ($2.00 \pm 0.13 \mu\text{M}$) [4].

For *in vivo* studies we chose choline zinc derivative ZnPcChol_8 as the most promising substance; on its basis, Holosens-lio agent was developed whose preclinical testing has been completed to date.

A series of 2,3-naphthalocyanine derivatives were subjected to *in vitro* studies.

There are four naphthalene rings conjugated with the macrocycle in 2,3-naphthalocyanines, which feature distinguishes them from their related compounds, phthalocyanines. The main absorption band of 2,3-naphthalocyanines lies in the 750–780 nm region; the singlet oxygen quantum yield is of the order of 0.45.

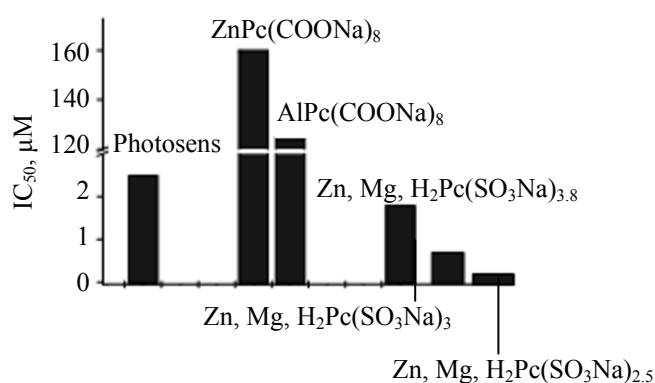


Fig. 1. Photoinduced cytotoxicity of phthalocyanine derivatives (IC_{50} , μM). HEP2 cell culture; incubation time 2 h.

Our studies revealed instability in biological media and low photoinduced activity towards cells in the culture ($\text{IC}_{50} \gg 200 \mu\text{M}$) for this class of photosensitizers, which made impracticable their further studies.

Synthetic Tetrahydroporphyrins (Bacteriochlorins)

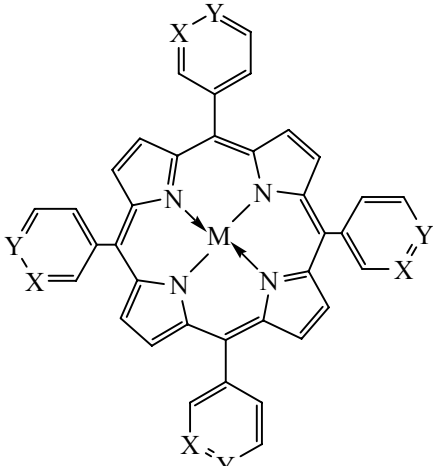
These compounds have an absorption maximum in the 740–760 nm region, and the molar absorption coefficient of $(7-8) \times 10^4 \text{ L mol}^{-1} \text{ cm}^{-1}$; the singlet oxygen quantum yield is 0.3–0.45. An advantage offered by these photosensitizers is hydrophilicity, making them applicable in the form of aqueous solutions. We studied tetrahydroporphyrin derivatives with different side substituents and central metal atoms (Table 3).

The absorption and fluorescence analyses showed that most of these dyes are stable over the selected time interval; three of the dyes, nos. **XXII**, **XXIV**, and **XXVI**, proved to be less stable. It was found that the

Table 2. Positively charged phthalocyanine derivatives

Comp. no.	Macrocycle	Substituent R	Central atom M	Designation
XIII		$-\text{CH}_2\text{N}^+\text{Me}_2\text{CH}_2\text{CH}_2\text{OH Cl}^-$	Zn	ZnPcChol_8
XIV		$-\text{CH}_2\text{N}^+\text{Me}_2\text{CH}_2\text{CH}_2\text{OH Cl}^-$	AlOH	AlPcChol_8
XV		$-\text{CH}_2\text{N}^+\text{Me}_2\text{CH}_2\text{CH}_2\text{OH Cl}^-$	HH	$\text{H}_2\text{PcChol}_8$
XVI		$-\text{CH}_2\text{N}^+\text{C}_5\text{H}_4\text{Cl}^-$	Zn	ZnPcPy_8
XVII		$-\text{CH}_2\text{N}^+\text{C}_5\text{H}_4\text{Cl}^-$	AlOH	AlPcPy_8

Table 3. Synthetic tetrahydroporphyrins (bacteriochlorins)

Comp. no.	Macrocycle	X	Y	Central atom M	λ_{\max} , nm
XVIII		$N^+(CH_2)_4Br Br^-$	CH	HH	765
XIX		$N^+(CH_2)_4N^+C_5H_5 2Br^-$	CH	HH	765
XX				Zn	778
XXI		$N^+(CH_2)_4N^+(CH_3)_2(CH_2)_2OH 2Br^-$	CH	HH	765
XXII		$N^+CH_2COOC_2H_5 Cl^-$	CH	HH	766
XXIII		$N^+CH_3 I^-$	CH	HH	761
XXIV		$N^+CH_3 n-CH_3C_6H_4SO_3^-$	CH	HH	763
XXV				Zn	775
XXVI		CH	$C-O(CH_2)_4N^+C_5H_5 Br^-$	H	740

zinc complex of tosyl derivative **XXV** undergoes degradation (as indicated by the lack of a long-wavelength peak in its fluorescence spectra), so this compound was not used in further experiments.

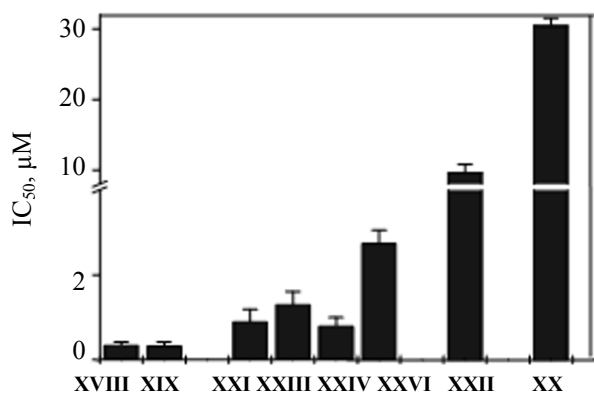
All the synthetic tetrahydroporphyrins tested by us exhibit no dark cytotoxicity against tumor cells in the

culture. The highest photoinduced cytotoxicity was found in tetra- (**XVIII**) and octacationic (**XIX**) metal-free derivatives. Introduction of the zinc atom into the macrocycle (**XX**) causes a strong (30–35-fold) reduction of the photoinduced activity of the photosensitizers (Fig. 2).

Among the synthetic tetrahydroporphyrins, the highest photodynamic efficacy against the cells in culture is exhibited by metal-free tetrabromide (**XVIII**) and octacationic (**XIX**) derivatives: IC_{50} 0.34 ± 0.07 and $0.37 \pm 0.08 \mu M$, respectively (Fig. 2) [5, 6]. *In vivo* screening (mice experiments) validated high photoinduced antitumor activity of these compounds towards Lewis lung carcinoma, with 100% recovery rate achieved in animals. Metal-free tetrahydroporphyrin derivatives (nos. **XVIII** and **XIX**) were recognized as promising candidates for further in-depth study.

5-Aminolevulinic Acid Hydrochloride (5-ALA) and Its Esters

By now, fairly extensive experience has been accumulated on the use of 5-ALA-based agents for fluorescence diagnosis and photodynamic therapy of malignant tumors of different localizations, as well as of nontumoral skin diseases [7–10]. A broad range of dosage forms were developed for administration of 5-

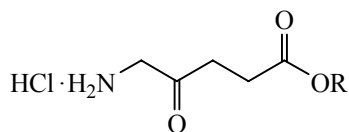


XVIII	$0.34 \pm 0.11 \mu M$	XXII	$9.71 \pm 1.20 \mu M$
XIX	$0.37 \pm 0.08 \mu M$	XXIII	$1.50 \pm 0.07 \mu M$
XX	$30.52 \pm 1.21 \mu M$	XXIV	$0.79 \pm 0.09 \mu M$
XXI	$0.75 \pm 0.08 \mu M$	XXVI	$2.75 \pm 0.12 \mu M$

Fig. 2. Photoinduced activity of synthetic tetrahydroporphyrins. Incubation time 2 h.

ALA-based agents by different routes: an ointment and a gel for applications in treatment of skin diseases and in gynecology; a sterile solution for instillation into the urinary bladder and bronchial administration; and an oral medication for gastric and esophageal cancer diagnosis and treatment. In recent years, Metvix and Hexvix (Norway) agents based on methyl and hexyl esters of 5-aminolevulinic acid, respectively, have been used for fluorescence diagnosis. Being more hydrophobic than the acid itself, the esters more efficiently overcome the biological membrane barriers and, thereby, more rapidly accumulate within the cells in larger amounts and get involved in biosynthesis as protoporphyrin precursors [11].

We synthesized methyl (ME-5-ALA) and hexyl (HE-5-ALA) esters of 5-ALA by the original technique.



R = H (5-ALA), CH₃ (ME-ALA), CH₃(CH₂)₅ (HE-ALA).

Both 5-ALA and its esters are biological precursors of protoporphyrin IX (PPIX). Their excess amount in the tumor cells leads to increased induction and accumulation of PPIX, which causes photodynamic damage of the cells when the lesion is irradiated with the light of a specific visible wavelength. Porphyrins give a low singlet oxygen quantum yield, so the implementation of the photodynamic effect requires more fluorochrome (in the present case, endogenous photoactive compound PPIX), in an amount determined by the number of the cells accumulating the photosensitizer. Considering the above-said, we examined the induced PPIX phototoxicity in relation to the plating density of the cell population during photodynamic action.

For example, under irradiation of the HEP2 culture cells at the plating concentration of 0.25×10^5 and 0.5×10^5 cells mL⁻¹ the PPIX mediated phototoxicity of the compounds was negligible; the greatest inhibitory effect on the culture growth under photodynamic action was observed at the plating concentration of 10^5 cells mL⁻¹. This dependence held both for HE-5-ALA and ME-5-ALA esters and for 5-ALA proper. The results are presented in Fig. 3, with 5-ALA hexyl ester as an example.

The outcome of photodynamic treatment also depends on the time of incubation of the cells with the

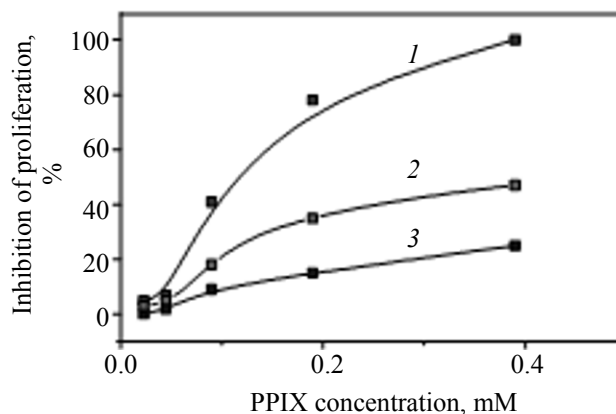


Fig. 3. The PPIX mediated phototoxicity for HE-5-ALA in relation to the inoculum density of HEp2 cells. (1) 10^5 , (2) 0.5×10^5 , and (3) 0.25×10^5 cell mL⁻¹. Incubation time 18 h.

photosensitizer (Table 4). For example, at the incubation time of 18 and 24 h the PPIX mediated phototoxicity was significantly higher than that observed at 6 h. Therefore, for convenience of the experiments, the 24-h time interval was selected for estimation of the specific activity of the substances. Among the compounds tested, the highest PPIX mediated phototoxicity against the cells in the culture was revealed for 5-ALA hexyl ester.

Based on the standard substance of 5-aminolevulinic acid hexyl ester, Hexasens-lio agent was developed for fluorescence diagnosis and photodynamic therapy; its preclinical testing has been completed to date.

Nanostructured Photosensitizers

One of the negative characteristics possessed by soluble phthalocyanines is their “long” pharmacokinetics. Slow excretion of phthalocyanines from the body can cause phototoxic reactions, above all cutaneous phototoxicity, which factor limits the application of phthalocyanines in many cases. These complications can be avoided by administering into the body a pro-drug, a substance lacking photoactive properties, activated by irradiation directly in the pathological focus area.

As pro-drugs we tested photoinert nanoparticles of crystalline phthalocyanines: aluminum phthalocyanine AlPc, zinc phthalocyanine ZnPc, and metal-free phthalocyanine H₂Pc. The nanoscale AlPc, ZnPc, and H₂Pc were transferred to the photoactive (molecular) state by irradiation with high-power laser pulses at a wavelength in the region of the nanoparticles absorption.

Table 4. The PPIX mediated phototoxicity of HE-5-ALA, ME-5-ALA, and 5-ALA (IC_{50} , mM) in relation to the time of incubation before irradiation

Compound	Incubation time, h			
	6	9	18	24
5-ALA	5.00±0.09	0.53±0.05	0.37±0.08	0.35±0.11
HE-5-ALA	1.60±0.11	0.42±0.07	0.27±0.07	0.25±0.06
ME-5-ALA	4.00±0.12	2.10±0.07	0.91±0.09	0.89±0.09

We studied the fluorescence and *in vivo* antitumor efficacy of the activated AlPc, ZnPc, and H₂Pc nanostructures; for dimensions of the nanoparticles in a 0.2% aqueous dispersion, see Table 5.

It was found that nanoscale AlPc, ZnPc, and H₂Pc in a 0.2% aqueous dispersion do not fluoresce, but after irradiation with 10 laser pulses they exhibit fluorescence of the molecular form with band maxima at 697 (AlPc), 679 (ZnPc), and 697 nm (H₂Pc). The fluorescence intensities were comparable for all the samples.

We carried out *in vivo* experiments in mice with S37 sarcoma, which was transplanted under the skin on the lateral surface of the femur of the animals after they were intravenously administered AlPc, ZnPc, and H₂Pc nanoparticles. No fluorescence characteristic for the molecular form of these compounds was observed both in the tumor and in different anatomical areas of the skin of the animals. After pulsed irradiation of the tumor lesion, fluorescence was detected, though in the area exposed to pulsed radiation solely, i.e., directly in the region of the tumor growth. Figure 4 shows the fluorescence spectra of ZnPc for the tumor lesion and the surrounding tissue in mice with S37 sarcoma.

The experiments on mice with S37 sarcoma, undertaken with the aim to assess the efficacy of photodynamic therapy with AlPc, ZnPc, and H₂Pc nanoparticles, revealed a pronounced antitumor action: complete resorption of the tumor, long-term inhibition of the tumor growth by 97–67%, and full recovery in

100–78% of the cases (Table 6). The best therapeutic effect was observed for the ZnPc and AlPc nanoparticles; pulsed and continuous-wave irradiation, when applied individually, did not lead to biologically significant inhibition of the tumor growth. In the case of H₂Pc nanoparticles, the photodynamic therapy was slightly less efficacious.

Thus, AlPc, ZnPc, and H₂Pc nanoparticles can be regarded as promising “pro-photosensitizers” for photodynamic therapy, which are activated under exposure to high-power laser pulses. Considering these data, as well as the manufacturability characteristics, ZnPc nanoparticles were selected for further in-depth studies.

Development of Original Agents for Fluorescence Diagnosis and Photodynamic Therapy and Their Preclinical Trials

In the screening stage, based on the results of the studies performed *in vitro* and *in vivo*, the following promising agents were selected: Alasens and Hexasens for fluorescence diagnosis, and Phthalosens, Holosens, ZnPc nanoparticles, and tetrabromide (XVIII) and octacationic (XIX) tetrahydroporphyrin derivatives (see Table 3), for photodynamic therapy. It should be noted that Holosens substance is also suitable for antimicrobial photodynamic therapy.

For Alasens, Hexasens, Phthalosens, and Holosens substances, drug dosage forms were developed, and their physicochemical and biological standardization was carried out. In development of dosage forms, account was taken of the routes and methods of administration of the agent (injection, oral, application), as well as of its composition and the form of use (preparation of a solution of the agent, presence of auxiliaries: solubilizers, fillers, stabilizers, and gelling agents). In development of the injectable form, the behavior of the agent in different solvents commonly used in medicine (saline, 5% glucose solution, rheopolyglukin, hemodes, etc.) was evaluated in order to choose the most appropriate form in which the agent exhibits the maximum sensitizing properties.

Table 5. Dimensions of the ZnPc, AlPc, and H₂Pc nanostructures A 0.2% dispersion in 0.9% NaCl solution, stabilized with Lutrol F127

Nanostructure size	ZnPc	AlPc	H ₂ Pc
Total size in dispersion, μm	0.08–0.38	0.06–0.38	0.13–0.86
Most probable diameter, μm	0.11±0.02	0.10±0.01	0.21±0.03
Average diameter, μm	0.16±0.02	0.15±0.01	0.27±0.02

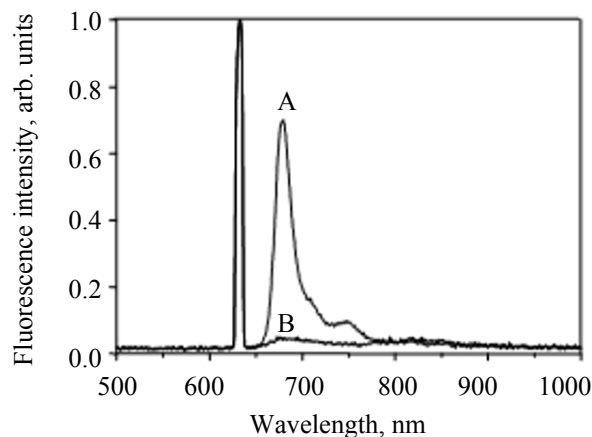


Fig. 4. Fluorescence spectra of ZnPc for the tumor lesion and the surrounding tissue in mice with sarcoma S37: (A) Spectrum from the zone exposed to high-energy laser pulse irradiation (at the tumor lesion) and (B) spectrum from the zone beyond the irradiated area (skin areas surrounding the tumor and distant skin areas).

Preclinical trials included studies of the specific activity (fluorescence and/or photoinduced antitumor efficacy), pharmacokinetics, and safety (acute, subchronic, and chronic toxicity; allergenic properties; local irritant effect, skin phototoxicity).

Alasens-lio and *Alasens-gel* are original drugs developed on the basis of 5-aminolevulinic acid, a precursor of endogenous photosensitizer protoporphyrin IX (PPIX), which possesses fluorescent properties. The latter accumulates in the tumor cells within several hours, and its high level is preserved for 1–2 h. In normal cells, PPIX is rapidly utilized via conversion to heme. The accumulation of PPIX in the tumor and fast utilization in normal tissues leads to a high, up to 10–15-fold, fluorescent contrast for different tumors. This contrast provides for neoplasm demarcation during fluorescence diagnosis and allows a local therapeutic effect to be produced without causing damage to the surrounding tissue.

The *Alasens-lio* dosage form is a crystalline powder, white to cream-colored, used as solutions for instillation, inhalation, and ingestion. As to *Alasens-gel*, this is an aqueous hydroxyethyl cellulose-based gel for external use [12–14].

Specific fluorescence of PPIX in the tumor tissues of the mice was observed during the first 6 h after oral administration of 500 mg kg⁻¹ *Alasens-lio*. For example, PPIX effectively accumulates in lymphocytic leukemia P388: The fluorochrome accumulation peak was observed 2 h after administration of 5-ALA; the

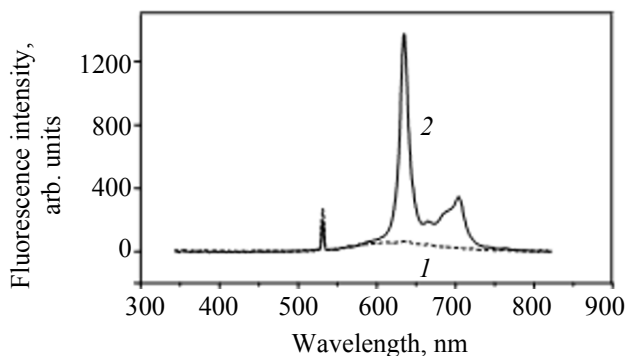


Fig. 5. The Ehrlich tumor fluorescence spectra: (1) before and (2) after 4-h *Alasens-gel* application.

intensity of the fluorescence signals in the tumor significantly exceeds that in the surrounding tissue (skin). Thereby, high fluorescence contrast between the tumor and the surrounding tissue (5.7 ± 1.9 arb. units) is achieved, which allows visualization of the tumor lesion. Further, the PPIX fluorescence signals decrease in intensity in the tumor and continue to increase in the skin, which leads to decreased fluorescence intensity ratio between the tumor and the surrounding tissue and reduced visual fluorescence contrast between them.

Tumors display different abilities for accumulating PPIX under the action of 5-ALA injected. The fluorescence signal in the tumor and the fluorescence contrast were the highest in the mice with LLC carcinoma (7.0 ± 3.0 arb. units) and P388 lymphocytic leukemia (6.0 ± 0.3 arb. units). The PPIX accumulation levels in Ehrlich tumor are significantly lower; the fluorescent contrast is 2–3.5 times lower, 3.0 ± 2.0 arb. units.

A pharmacokinetic study by local fluorescence spectroscopy of *Alasens-lio* at the dose of 500 mg kg⁻¹ administered systemically to intact mice revealed two-peaked 5-ALA-induced PPIX fluorescence with maxima at 635 and 703 nm, characteristic for PPIX fluorescence in tissues. The 5-ALA-induced fluorescence in the mice is recorded during the first hours of observation. The accumulation levels of endogenous porphyrins in the epithelial tissues are higher than those in the muscle tissue. When administered systemically to healthy mice, *Alasens-lio*

Table 6. Antitumor efficacy of photodynamic therapy method with AlPc, ZnPc, and H₂Pc nanostructures. Experimental animals: mice with S37 sarcoma. Treatment was started on day 6–7 after tumor inoculation

Pulse (“activation”) irradiation parameters	Continuous irradiation parameters	Tumor growth inhibition, %					Life span, %	Recovery rate, %
		days post-treatment						
		9	13	16	18	20		
ZnPc nanostructures, 15 mg kg ⁻¹								
0.6 J cm ⁻² pulse ⁻¹ 6 J cm ⁻² (10 pulses)	100 mW cm ⁻² 90 J cm ⁻²	100 ^a	100 ^a	100 ^a	100 ^a	100 ^a	—	100
0.6 J cm ⁻² pulse ⁻¹ 6 J cm ⁻² (10 pulses)	—	39	27	19	20	6	0	0
—	100 mW cm ⁻² 90 J cm ⁻²	47	29	25	25	27	0	0
AlPc nanostructures, 15 mg kg ⁻¹								
0.6 J cm ⁻² pulse ⁻¹ 6 J cm ⁻² (10 pulses)	100 mW cm ⁻² 90 J cm ⁻²	100 ^a	100 ^a	100 ^a	100 ^a	95 ^a	35 ^b	78
0.6 J cm ⁻² pulse ⁻¹ 6 J cm ⁻² (10 pulses)	—	36	22	14	5	2	0	0
—	100 mW cm ⁻² 90 J cm ⁻²	22	31	19	9	4	0	0
H ₂ Pc nanostructures, 15 mg kg ⁻¹								
0.6 J cm ⁻² pulse ⁻¹ 6 J cm ⁻² (10 pulses)	100 mW cm ⁻² 90 J cm ⁻²	100 ^a	100 ^a	97 ^a	87 ^a	67 ^a	48 ^b	0
0.6 J cm ⁻² pulse ⁻¹ 6 J cm ⁻² (10 pulses)	—	55 ^a	46 ^a	46	44	26	0	0
—	100 mW cm ⁻² 90 J cm ⁻²	37	42	24	18	26	0	0

^a The average tumor size in the mice from the experimental group was significantly different from that in the control group at $p < 0.05$.

^b The average life span of the mice from the experimental group was significantly different from that in the control group at $p < 0.05$.

causes an increase in the endogenous porphyrin levels in all tissues except for cerebral cortex. The fluoro-chrome accumulation level in the skin was at a maximum 4 h after the drug administration, and after 24 h the PPIX fluorescence in the skin did not differ from the normal levels. Endogenous porphyrins were excreted from the body of healthy mice within 24 h. The primary routes of elimination of PPIX resulted from the drug administration are by the kidneys into the urine and by the liver into the bile.

Based on the results obtained, a clinical trial protocol was developed for Alasens-lip useful in fluorescence diagnosis of malignant tumors of skin, bladder, trachea, bronchi, mucous membranes of the mouth and digestive tract, and early endometrial cancer, as well as for photodynamic therapy of malignant tumors of skin, bladder, and prostate.

Another dosage form developed by us on the basis of 5-aminolevulinic acid for local application purposes is Alasens-gel; this form is more convenient than Alasens-ointment for dermatological and gynecological applications in clinical practice.

When used as skin application, Alasens-gel leads to fluorescence from the application zone with the maxima at 635 and 705 nm, characteristic for PPIX (Fig. 5).

In the case of Ehrlich tumor, the induced fluorescence tends to increase in intensity with the time of gel application increasing from 1 to 6 h in all the layers of the tumor. Twenty-four hours after application of the gel the fluorescence intensity was not significantly different from the background. A significant difference between the control and experiment in the superficial

Table 7. Antitumor efficacy of photodynamic therapy (PDT) with Alasens-gel

Effect	Tumor growth inhibition,%						
	observation time, days						
	6	8	10	13	15	17	20
Ehrlich tumor							
PDT with Alasens-gel	75	77	89	80	75	63	45
Alasens-gel	17	27	11	29	40	44	–12
Sarcoma S37							
PDT with Alasens-gel	67	60	52	52	30	10	10
Alasens-gel	10	16	15	27	12	10	5

tumor layers was recorded 2 h, and in deeper layers, 4 h after application of the gel.

The distribution of induced PPIX in the tissues of the mice with transplantable tumors was examined 4 h after application of 0.1 mL cm^{–2} of Alasens-gel. The induced fluorescence levels observed after 4-h application of the gel in all the tumors examined (Ehrlich, S37, LLC, C26) were comparable.

With Alasens-gel, the PPIX accumulation is observed not only for superficial but also for up to 5 mm-deep layers of tumor, which evidences high permeability of tissues to 5-aminolevulinic acid as part of aqueous gel.

Comparison of the fluorescence intensities measured for different tumors showed that, in the LLC, S37, and C26 tissues, PPIX is distributed more uniformly than in Ehrlich tumor. The reason is higher vascularization and a more uniform distribution of blood vessels in LLC, S37, and C26 tumors compared to Ehrlich tumor. It should be noted that the acid is released from the gel and, after passing through the skin, gets involved in the local blood flow which carries it across the tumor.

The pharmacokinetic study by the spectroscopic method showed that fluorescence was excited in virtually all the organs examined, except for the brain, with the spectrum exhibiting two peaks characteristic for PPIX, at 635 and 705 nm. The highest fluorescence level was recorded for small intestine, and the lowest, for adrenal glands. Twenty-four hours after application of Alasens-gel weak induced fluorescence signals were recorded in skin and in bladder. In other organs and tissues the fluorescence levels did not exceed the background values.

Photodynamic therapy with Alasens-gel causes inhibition of Ehrlich tumor and S37 sarcoma growth, with therapeutic effect (tumor growth inhibition TPO³ 50%) detectable within 2 weeks after the treatment. Without further radiation exposure, Alasens-gel does not stimulate tumor growth (Table 7). Regardless of the therapeutic effect, photodynamic therapy with Alasens-gel provides an excellent cosmetic effect due most likely to inhibition of collagen, which prevents formation of rough scars.

Hexasens-lio is an original agent developed on the basis of 5-aminolevulinic acid hexyl ester (HE-5-ALA). This is a lyophilisate comprised of 10 mg of HE-5-ALA and 40 mg of sodium chloride. An inducer of porphyrin synthesis in biological objects, *Hexasens-lio* causes in the tumor cells and tissues fluorescence whose spectrum is characteristic for PPIX in terms of both the shape and position of peaks (630 and 750 nm).

A 2-h exposure to the agent (0.02 mg) leads to high production of PPIX in the rabbit urinary bladder epithelium (diagnostic fluorescent parameter Df 3.6 ± 1.4 arb. units), whose decrease correlates with that in the drug dose: Introduction of 0.01 mg led to a decrease in the specific fluorescence intensity of the fluorochrome by a factor of 1.6 and to its nonuniform synthesis (Df 2.2 ± 0.9 arb. units).

Comparison of the effects produced by *Hexasens-lio* and *Alasens-lio* as PPIX inducers showed that, in the case of intrabladder administration of 0.02 mg of a 0.002% solution of *Hexasens*, the fluorescence level is comparable to that achieved with intrabladder administration of 300 mg of a 3% aqueous solution of *Alasens*. Thus, HE-5-ALA is an extremely efficacious agent for fluorescence diagnosis [11].

Table 8. Antitumor efficacy of photodynamic therapy with Phthalosens-lio with respect to tumors of different geneses

Tumor	Tumor growth inhibition, %					Life span ^a , %	Recovery rate ^b , %
	observation time, days						
	7	9	11	14	16		
LLC	100	100	100	100	100	250	100
C26	100	100	100	100	100	57	33
S37	96.7	89.4	86.8	83.6	79.5	47	43
P388	100	100	91.3	92.1	90.2	31	0
B16	100	99.0	97.8	91.7	84.5	32	0

^a Phthalosens-lio dose 0.5 mg kg⁻¹; time interval between Phthalosens-lio administration and irradiation exposure 2 h; radiation energy density 270 J cm⁻². ^b Recorded on day 90 of observation.

It should be noted that a 2-h intrabladder instillation of Hexasens-lio even at a higher concentration (0.01%) resulted in PPIX induction only in the rabbit bladder epithelium ($D_f 5.4 \pm 0.4$ arb. units). At the same time, specific PPIX fluorescence in the internal organs was lacking, which evidences that, when administered by the intrabladder instillation, the agent does not enter the systemic blood flow.

Hexasens induces fluorescence in murine primary and metastatic tumor foci. Among tumors of different geneses [epithelial (Ehrlich tumor, LLC, and C26) and nonepithelial (P388 and S37)], the highest fluorescence contrast relative to the primary focus is observed in the mice with LLC tumor (3.3 ± 0.9 to 5.3 ± 2.4 arb. units), and the lowest, in the mice with Ehrlich tumor (1.6 ± 0.4 to 1.7 ± 0.5 arb. units). A high level of the HE-5-ALA-induced fluorescence was also recorded in lung metastases of carcinoma C26 and LLC. In the surrounding tissues, this level is lower than that in the metastases. The highest fluorescent contrast between the tumors and normal tissues appears in early stages of observation, from 0.5 to 2 h, primarily 1 h after oral administration of 500 mg kg⁻¹ of the agent.

Photodynamic therapy with Hexasens leads to long-term tumor growth inhibition. For example, in the mice with S37 sarcoma, TGI of 75–100% was observed during the 12-day period that followed the treatment with 125–250 mg kg⁻¹ of Hexasens (radiation energy density 360 J cm⁻², time interval between introduction of the agent and radiation exposure 1 h).

Study of the Hexasens-lio safety showed that this is a low-toxicity drug which exerts no toxic effect on

peripheral blood, liver, kidneys, and gastrointestinal tract organs. When administered into the bladder at $\leq 0.01\%$ concentrations, an aqueous solution of Hexasens-lio produces no local irritant action [15].

Based on the results of the preclinical trials of Hexasens-lio, “A Controlled Open-Label Study to Evaluate the Tolerability and Diagnostic Efficacy of Hexasens-Lio for Fluorescence Diagnosis of Bladder Cancer” protocol was developed.

Phthalosens-lio is an original agent comprised of a mixture of sulfonated phthalocyanines with the average degree of sulfonation of ~ 2.5 (IV in Table 1). The dosage form of Phthalosens-lio is lyophilisate for solution for injection.

Phthalosens-lio accumulates in tumors of different geneses (P388, LLC, S37, C26, and B16) and in the surrounding tissue. The accumulation level of the drug in tissues was determined from its normalized fluorescence by local fluorescence spectroscopy. The normalized fluorescence maxima were recorded in tumors of different geneses 0.5–4 h after the drug administration. In this time interval, the fluorescent contrast relative to the surrounding tissue is 3.5–5.0 (skin) and 1.3–4.0 (muscle) arb. units, depending on the morphological structure of the tumor [16].

A maximum therapeutic effect is produced by irradiation 2 h after administration of 0.5 mg kg⁻¹ Phthalosens at the radiation energy density of 90 J cm⁻² (TGI 90–100%). Photodynamic therapy conducted under optimal conditions demonstrated high antitumor efficacy of Phthalosens against all the tumors examined (Table 8). The best results were obtained for LLC carcinoma (100% recovery rate), as well as for colon adeno-

carcinoma C26. A comparative analysis showed that, for Phthalosens-lio, the effective doses are 5–8 times lower than those for Photosens [17].

Photodynamic therapy with Phthalosens causes inhibition of the tumor metastasis process (the inhibition index of LLC metastasis is $25.5 \pm 3.5\%$).

Pharmacokinetic studies by the local fluorescence spectroscopy method showed that, when administered at therapeutic doses, Phthalosens-lio enters various organs and tissues in animals within 5–15 min. After 3 days, the drug is eliminated from liver and spleen by ~90%, and from the remaining organs (kidney, skin, muscle, adipose tissue), by ~50%. Trace amounts of Phthalosens-lio are detectable in skin, liver, kidneys, and spleen during 1.5 months. Fluorescence analysis indirectly evidences that the main elimination route for Phthalosens-lio from the animal body is through kidneys with urine [17].

Preclinical examination of the general toxic properties of Phthalosens-lio, including acute and chronic toxicity in mice, rats, rabbits, and dogs, as well as of specific types of toxicity (allergic effects, immunotoxicity) revealed good tolerability by animals administered Phthalosens-lio at doses exceeding 50–750 times the human equivalent doses. At the doses tested, Phthalosens-lio had no pronounced irreversible toxic effects on peripheral blood, liver, kidneys, organs of the gastrointestinal tract, central nervous system, and immune system of the animals. Toxic and side responses identified (dystrophic and destructive changes in the liver and kidneys of the dogs) were moderate, dose-dependent, and reversible, and were found only for chronic Phthalosens administration at doses exceeding 50 and 100 times the human equivalent dose [18].

Comparison of the skin phototoxicity caused by Phthalosens and its nearest analog Photosens applied in the therapeutic irradiation regimes showed that, during the photodynamic therapy session, skin photodamages were identical. However, 7 days after administration of the drugs in therapeutic doses, the skin phototoxicity caused by Phthalosens was significantly lower than that for Photosens. Compared to Photosens, Phthalosens-lio causes less prominent skin phototoxic effects of shorter duration [19].

Based on the results obtained, “A Prospective Open-Label Study to Evaluate the Tolerability and Efficiency of Phthalosens-Lio as a Photosensitizer for

Fluorescence Diagnosis and Photodynamic Therapy in Patients with Basal Skin Cancer” protocol was developed.

Holosens-lio and *Holosens-gel* are original agents comprised of the choline derivative of zinc phthalocyanine (**XIII** in Table 2).

Examination of the distribution of Holosens-lio in the animals with transplantable tumors, performed by the local fluorescence spectroscopy method, showed that the drug accumulates in C26, LLC, S37, and B16 tumors. The normalized fluorescence level depends on the time elapsed since administration of Holosens-lio; for all the tumors it reaches a maximum (from 6.7 ± 0.6 to 10.7 ± 2.4 arb. units) 15–60 min after administration and subsequently decreases fairly rapidly. The normalized fluorescence level for the tumor tissues after 72 h is 19.5% of the maximum value (in the case of LLC carcinoma). Holosens-lio is retained for the longest time in tumor S37, and its elimination is the fastest in the case of B16 tumor [21].

The Holosens-lio photosensitizer has a tropism toward tumor tissue. The fluorescent contrasts relative to skin and muscle for the tumors studied are close: from 2.0 ± 0.2 to 3.4 ± 0.6 and from 2.2 ± 0.4 to 3.7 ± 0.9 arb. units, respectively, in the 15–60 min range.

The following therapeutic regimes for photodynamic therapy with Holosens-lio were determined: drug dose $0.5\text{--}1.0 \text{ mg kg}^{-1}$, time interval between the drug administration and radiation exposure 15–30 min, and energy radiation density $90\text{--}180 \text{ J cm}^{-2}$ (irradiation with an LED source, wavelength maximum 685 nm) and drug dose 0.5 mg kg^{-1} , 15-min interval, and energy radiation density $90\text{--}180 \text{ J cm}^{-2}$. In these regimes, excellent results can be achieved in treatment of tumors of different geneses (Table 9). The highest treatment efficacy was observed for LLC, C26, and S37 tumors, with the average life span of the animals increased by 115.3, 109.3, and 121.0%, respectively, and the recovery rate, by 66.7, 25, and 40%, respectively. The lowest efficacy was achieved in the case of B16 tumor, specifically, tumor growth inhibition of 51.4–80.9%, no recovered animals, and biologically insignificant increase in the life span [21].

The pharmacokinetic studies showed that Holosens-lio instantly enters the internal organs and tissues of the animals, whereupon it is slowly eliminated. The drug in the monomeric form accumulates predominantly in liver and bladder and is eliminated from the muscle, adipose tissue, kidney, bladder, and lungs

Table 9. Antitumor efficacy of photodynamic therapy with Holosens-lio with respect to tumors of different geneses

Tumor	Tumor growth inhibition, %					Life span ^a , %	Recovery rate ^b , %
	observation time, days						
	8	11	13	15	18		
LLC	98.0	90.7	90.2	86.2	88.7	115.3	66.7
C26	90.2	86.0	89.2	86.2	81.8	109.3	25.0
S37	98.6	98.1	93.9	94.0	92.1	121.0	40.0
B16	76.8	80.9	76.5	68.7	51.4	7.3	0

^a Time interval between Holosens-lio administration and radiation exposure 15 min; radiation power density 100 mW cm⁻²; radiation energy density 90 J cm⁻². ^b Estimated in the 120-day range.

by >90% over one day. An insignificant amount of Holosens-lio (4.6%) is detectable in skin within 1 month. Residual amounts of Holosens are detected in liver (8.9%) and spleen (20.8%) for over three months. The main route for the drug elimination from the animal body over one day is through the kidneys with the urine, and that for the residual amount, through the liver with the bile.

Preclinical examination of the general toxic properties of Holosens-lio, including acute and chronic toxicity in mice, rats, and rabbits, as well as of specific types of toxicity demonstrated good tolerability by the animals administered Phthalosens-lio at doses exceeding 50–450 times the human equivalent doses. Holosens-lio exerted no pronounced irreversible toxic effect on peripheral blood, liver, kidneys, organs of the gastrointestinal tract, and central nervous system of the animals. Toxic and side responses identified in the peripheral blood, liver, and kidneys of the rabbits were moderate, dose-dependent, and reversible, and were found only for chronic Holosens-lio administration at doses exceeding 100 times the human equivalent dose.

When administered at therapeutic doses, Holosens-lio exhibits low skin phototoxicity in mice; a minimal skin response (a weakly pronounced edema) was detected in the animals irradiated on day 7 after Holosens administration, regardless of the dose.

Along with high antitumor activity, Holosens-lio possesses strong antimicrobial properties for *Helicobacter pylori*, *Campylobacter jejuni*, *Escherichia coli* 1257, *Escherichia coli* 675, *Enterococcus faecalis*, *Staphylococcus aureus*, etc. [20]. With Holosens-lio used at the concentration of 1.2 μM, the multiplicity of infection caused by the experimental bacterial

suspension decreased by a factor of 10⁵. In view of the antimicrobial properties possessed by Holosens substance, Holosens-gel useful for antimicrobial photodynamic therapy was developed on its basis.

The accumulation of Holosens-gel in the wound, the surrounding tissues (skin, muscle), internal organs, and blood of the animals was studied [22, 23]. The accumulation level was estimated by local fluorescence spectroscopy from the normalized fluorescence level of the photosensitizer in relation to the content of the active substance in the gel composition (0.002, 0.01, 0.02, 0.05, 0.1, and 0.2%), which was used as a 2-h application over the surface of uninfected wound. In this case, the active substance (Holosens), regardless of its content, is localized predominantly in the wound and the surrounding tissue. In the bloodstream, only 0.2% of the active substance was detected. The optimal content of the active substance is that in gels containing 0.01–0.1% Holosens. When localized in wound, they exhibit intense fluorescence (from 30.6 ± 4.7 to 77.1 ± 3.9 arb. units).

The optimum time for application of “Holosens-gel 0.01%” agent (with the optimum content of the active substance) over the wound surface is 1–2 h; intense fluorescence (from 27.7 ± 6.5 to 30.6 ± 4.7 arb. unit) is recorded in the wound tissues, and no Holosens is detected in remote skin and muscle areas.

Visual macroscopic assessment of the influence of photodynamic therapy on uninfected wounds in the mice showed that irradiation after application of “Holosens-gel 0.01%” (with the optimum content of the active substance) does not cause spontaneous infection in both experimental and control groups; in the uninfected wounds, dermal toxicity is not

developed. The healing time is independent of the radiation energy density in the 7.5–22.5 J cm⁻² range.

Other promising photosensitizers for photodynamic therapy can be found in nanostructured zinc phthalocyanine ZnPc and metal-free synthetic tetrahydroporphyrins (Table 3, tetrabromide and octacationic derivatives, **XVIII** and **XIX**, respectively), which are currently undergoing thorough preclinical testing.

Nanostructured ZnPc was used for development of Nanosens agent intended for photodynamic therapy of malignant neoplasms. Preclinical trials on mice with S37 sarcoma showed that the therapeutic effect of photodynamic therapy with ZnPc nanoparticles depends on the parameters of the activating pulsed laser radiation, nanoparticles dose, and interval between the pulsed and continuous-wave laser radiation exposure of the tumor lesion, as well as on the continuous-wave irradiation parameters. The most pronounced antitumor effect was achieved at the radiation energy density of 6 J cm⁻²: In the mice with S37 sarcoma, complete resorption of the tumor lesion was observed within 7 days after treatment, along with full recovery in 15% of the mice, long-term (20-day post-treatment period) inhibition of the tumor growth by 98–82%, and a survival rate increase by 39% with continued growth of the tumor.

The antitumor efficacy of photodynamic therapy with nanoparticles tended to increase with increasing nanoparticles dose from 1 to 15 mg kg⁻¹ and with decreasing time interval between the “activation” of the nanoparticles and the therapeutic procedure from 24 h to 2–5 min. The maximum dose of 15 mg kg⁻¹ the nanoparticles, subsequently “activated” in the tumor lesion after 2–5 min, provided for a very high treatment efficacy, specifically, full recovery of all the mice in the experimental group.

The most efficacious continuous-wave irradiation of the tumor lesion was achieved in the “low-intensity” mode, when inhibition of the tumor growth by 92–70% (*p* < 0.05) was detected in the mice with S37 sarcoma in this experimental group, which effect was detectable during a 20-day post-treatment period. The life span increased by 48%; full recovery was recorded in 84% of cases.

Tests on the mice with S37 sarcoma showed that the optimal therapeutic scheme for photodynamic therapy with ZnPc nanocomposites is as follows: intravenous injection of 7–15 mg kg⁻¹ of nanostruc-

tured ZnPc, 2–5 min → “activating” pulsed irradiation (radiation energy density per pulse no lower than 0.6 J cm⁻², number of pulses 5–10), 2–5 min → photodynamic therapy (radiation power density 10 mW cm⁻², radiation energy density 40 J cm⁻²).

Metal-free tetrabromide and octacationic derivatives of tetrahydroporphyrin (**XVIII** and **XIX**, respectively) are promising photosensitizers for development of a new-generation drug for photodynamic therapy of malignant tumors, which has no analogs so far.

Experimental study of the antitumor action of these photosensitizers was performed on mice with LLC carcinoma, inoculated subcutaneously to the outer surface of the femur. It was shown that both photosensitizers are accumulated in the LLC tumor tissue. The normalized fluorescence in the LLC tumor and the fluorescence contrast relative to skin and muscle were at a maximum 15 and 30 min after administration of compound **XVIII** and **XIX**, respectively. Based on these data, photodynamic therapy regimes were developed for tetrahydroporphyrin derivatives.

The photoinduced antitumor activity was evaluated *in vivo* in relation to the photosensitizer dose (2.5–5.0 mg kg⁻¹). Irradiation was performed on day 7 of the tumor growth during the period of the photosensitizer accumulation in the LLC tumor tissue (30 min after injection). Within 1 h after the radiation exposure, regardless of the light dose, the animals developed edema which persisted for prolonged time (for up to 15 days.). Both photosensitizers displayed a dose-dependent antitumor efficacy (Table 10). For example, the therapy with tetrabromide derivative no. 18 at the dose of 2.5 mg kg⁻¹ caused 70.9–100% tumor growth inhibition; the increase in the life span was not biologically significant, and no animals recovered; at the dose of 5.0 mg kg⁻¹, 100% inhibition of tumor growth and 100% recovery rate were achieved for the animals. With octacationic derivative **XIX** at the dose of 2.5 mg kg⁻¹, TGI of 94.1–100%, life span of 135.8%, and recovery rate of 66.7% were achieved; after increasing dose to 5.0 mg kg⁻¹ the efficacy increased: 100% TGI and 100% recovery rate.

The fluorescence of compound **XVIII** and **XIX** was at a maximum in the blood immediately after injection, and after 48 h it was not observed. Within 30 min, the fluorescent form of the tetrahydroporphyrin derivatives entered the internal organs and tissues of the animals; it predominantly accumulated in the liver and kidneys

Table 10. Photoinduced antitumor activity of the synthetic tetrahydroporphyrins towards carcinoma LLC^{a,b}

Comp. no.	Dose, mg kg ⁻¹	Tumor growth inhibition, %						Life span, %	Recovery rate, %	Death from toxicity, %
		day 7	day 9	day 11	day 14	day 16	day 18			
XVIII	2.5	100	98.3	92.5	90.0	87.7	70.9	14.6	0	0
	3.75	100	100	100	100	98.2	94.4	48.5	33.3	0
	5.0	100	100	100	100	100	100	—	100	0
XIX	2.5	100	97.5	95.6	94.4	94.1	95.4	136	66.7	0
	5.0	100	100	100	100	100	100	—	100	0

^a Time of observation of the animals 120 days. ^b Irradiation with an LED source, 759 ± 18 nm (radiation power density 100 mW cm⁻²).

and was subsequently eliminated from the organs and tissues at different speeds.

The residual amount of metal-free tetrahydroporphyrin **XVIII** and **XIX** administered at the effective dose of 5.0 mg kg⁻¹ was detectable in the spleen during 5 and 15 days, respectively, and in the liver and kidneys, during 40 days. The data obtained provide an indirect evidence for predominant elimination of the dye through the kidneys in the urine and through the liver in the bile of the mammals.

Compound **XVIII** and **XIX** exhibited a maximum fluorescence in the skin 0.5 and 4 h after their administration, respectively, whereupon the normalized fluorescence decreased. The residual amount of these dyes (6–8% of the maximum) in the skin was detectable for up to 20 and 25 days after administration, respectively (which indicates prolonged accumulation of the dyes in the skin), in the muscle, for up to 10 and 20 days, respectively, and in the adipose tissue, for up to 5 and 15 days, respectively.

A skin phototoxicity examination showed that the animals exposed to radiation on day 7 and day 28 after administration of the both tetrahydroporphyrin derivatives displayed a minimal skin response (a weakly pronounced edema). No deep skin damages were revealed. The presence of background fluorescence in the skin had no significant effect on the skin phototoxicity of the photosensitizers which is less prominent in the case of the tetrabromide and octacationic tetrahydroporphyrin derivatives than in the case of phthalocyanines (Photosens, Phthalosens, and Holosens).

Action Mechanism Study for New Photosensitizers

The efficiency of photodynamic action depends on a number of factors, including the level of accumulation and distribution of the photosensitizer in cellular

and tissue targets. The chemical properties of the photosensitizer determine its activity under the radiation exposure, the ability to bind to the intracellular organelles (mitochondria, lysosomes, Golgi apparatus) and to the macromolecular carriers in the bloodstream, and the ability to overcome biological barriers and identify specific targets. The level of the photosensitizer accumulation in the walls of blood vessels, stroma, or parenchyma of the tumor may determine the preferential target to be hit and, thereby, the photodynamic therapy efficacy. The ratio of the levels of accumulation of the photosensitizer in the tumor and adjacent normal tissues determines the selectivity of the damaging effect and the overall clinical response to therapy.

Using confocal microspectroscopy and reconstruction of spectral images (COMIRSI) on tumor cells, the Phthalosens and Holosens distribution in the tumor cells and in the tumor tissue was examined. This allowed not only obtaining quantitative information on the content of the photosensitizer in the target but also differentiating the origin of the fluorescence in individual tissue compartments. It was found that Phthalosens penetrates the tumor cells of different geneses (HEp2, A549, Raji) and accumulates therein in the monomeric (fluorescent) form, via being diffusely distributed in the cell cytoplasm and getting partially bound to the plasma membrane. No penetration of the photosensitizer in the cell nuclei was observed.

Also studied was the interstitial localization of Phthalosens on sections of C26 murine colon adenocarcinoma removed ex vivo at different times after intravenous administration (5, 15, and 30 min and 2, 4 and 24 h). Intense specific fluorescence of the dye, detected on the sections, indicated the presence of the monomeric form of the photosensitizer in the tissues (Fig. 6).

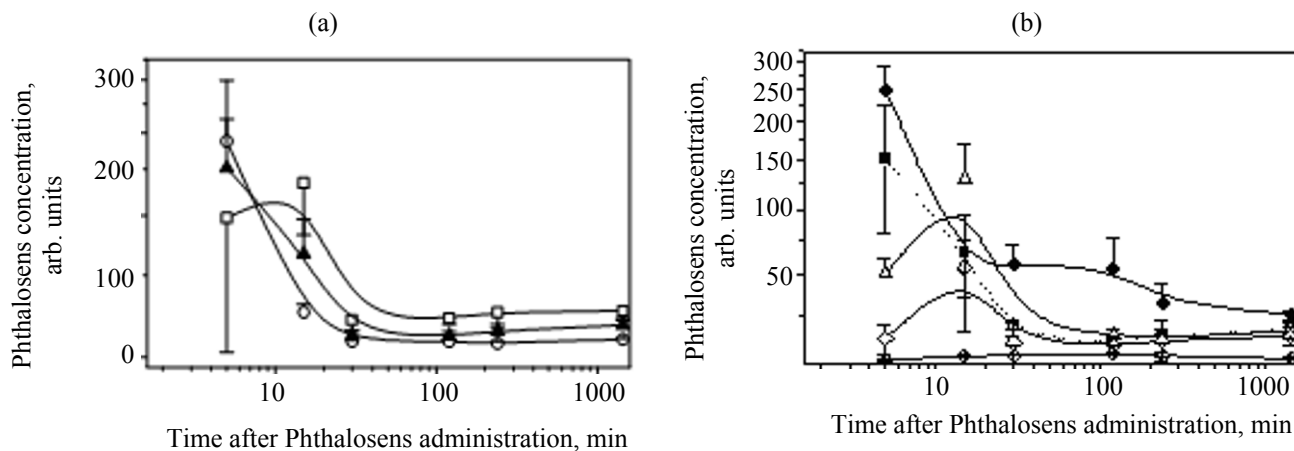


Fig. 6. Dynamics of the Phthalosens concentration in murine colon adenocarcinoma C26. The tumor was inoculated subcutaneously: in (open circles) central parts and (open squares) peripheral areas of the tumor lesion [(black triangles and squares) average whole tumor concentration], (black circles, dotted line) wall of blood vessels, (open triangles) connective tissue surrounding the tumor, (open diamonds) skin, and (open circles) muscle. The data are presented as $M \pm m$.

Analysis of the Phthalosens distribution dynamics within 24 h after intravenous administration at the dose of 1 mg kg^{-1} showed that, already within 5 min after administration, the photosensitizer penetrates efficiently into the tumor tissue and tumor cells. Within 15 min it gets localized in blood vessel walls, the tumor cells, and the connective tissue surrounding the tumor. However, in this period its distribution in the tumor is extremely heterogeneous. Subsequently, its concentration progressively decreases in the tissues, but the distribution becomes more homogeneous. The Phthalosens content in the blood vessel walls remained virtually unchanged over the period from 30 min to 2 h after administration. The greatest ability for accumulating Phthalosens is displayed by actively proliferating cells and, possibly, cells possessing macrophage activity.

Thus, when intravenously administered in tumor-bearing animals (LLC) at the therapeutic dose (1 mg kg^{-1}), Phthalosens rapidly enters the tumor lesion, wherein its initial level is maintained within 2–4 h. During this period the drug enters the vessels and subsequently penetrates from them into cancer cells and stromal elements in large amounts, whereupon its elimination begins.

The tissue distribution pattern derived suggests that the antitumor effect of photodynamic therapy with Phthalosens can be exerted both via antivasculature and direct cytotoxic and stroma-destructive actions.

The Holosens accumulation in the tumor lesion and the adjacent nontumor structures depends on the time

after administration. The fluorescence intensity in the tumor cells is lower than those in the blood vessel wall and in the dermis within the first few minutes after administration of the photosensitizer. The concentration of Holosens administered at the dose of 1 mg kg^{-1} achieves a maximum in the tumor cells 30 min after administration, whereupon it tends to slowly decrease. The normal muscle tissue, the epidermis, and the surrounding connective tissue exhibit weak accumulation of Holosens.

As follows from the tissue distribution data, the antitumor effect of photodynamic therapy with Holosens can be exerted both via antivasculature and direct cytotoxic and stroma-destructive actions.

Using the technique, developed by us on the basis of the COMIRSI methodology, for studying the kinetics of photosensitizer distribution in transplantable animal tumors, the Alasens and Photosens distribution in the tumor tissues of patients with basal-cell skin cancer was examined.

As shown by the study of the interstitial distribution kinetics of Alasens-induced protoporphyrin IX in the tumor and unaltered tissues, it accumulates in the tumor cells during the first few hours after administration of Alasens, whereby the intracellular synthesis of PPIX is indicated. The maximum concentration of Alasens in the tumor cells was recorded 2 h after oral administration of the drug. Subsequently, PPIX is redistributed, and after 6 h it is detected in equal amounts in the cells and stroma of the tumor. Throughout the study period the PPIX content in the

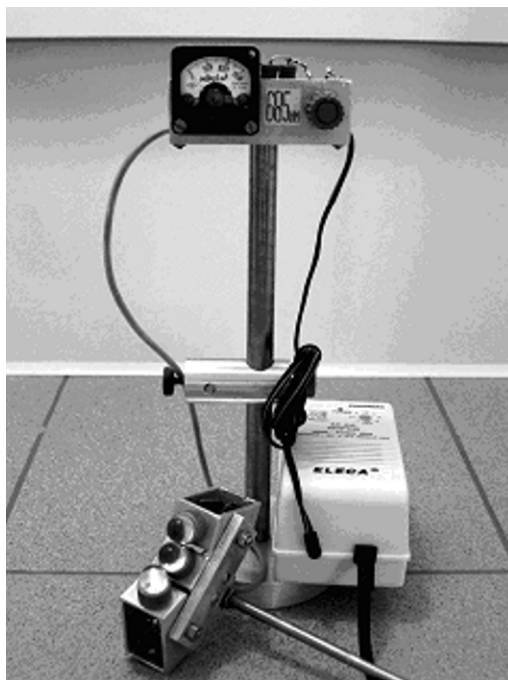


Fig. 7. An LED light source ($\lambda = 685$ nm) for photodynamic therapy.

unaltered skin and blood vessels was significantly lower than that in the tumor. These findings suggest a high fluorescence contrast and the possibility to achieve selective tumor necrosis by application of photodynamic therapy 2–6 h after administration of Alasens, with direct cytotoxic effect being the dominating mechanism of the tumor destruction.

A study of the interstitial distribution kinetics for Photosens revealed a lower tumor/norm fluorescent contrast. At the same time, throughout the survey the accumulation levels in the stroma exceeded those in the tumor cells. Ischemic necrosis is the predominant mechanism of the tumor destruction as a result of photodynamic therapy with Photosens. Especially pronounced ischemic changes can develop in the first 1–4 h after intravenous administration, during which period high Photosens content is recorded, in particular, in unaltered vessels.

Development of Optical Radiation Sources for Photodynamic Therapy

For all classes of the photosensitizers studied, optical radiation sources for experimental photodynamic therapy sessions were developed on the basis of LEDs with fixed or adjustable power density and different wavelengths: 640 ± 14 , 660 ± 16 , 670 ± 16 , 685 ± 16 , 720 ± 16 , 740 ± 14 , 760 ± 18 , and $800 \pm$

21 nm. These sources are the prototypes of facilities for clinical use. They enable screening of photosensitizers and adequate *in vitro* and *in vivo* studies of the photoinduced antitumor activity.

Figure 7 shows, by way of example, the LED light source for photodynamic therapy with Phthalosens and Holosens. It consists of three LEDs (divergence angle 8°) with a regulator of the radiation power from 25 to 150 mW cm^{-2} . The light dose ranges from 45 to 300 J cm^{-2} , the light spot diameter, from 1.0 to 1.5 cm, and the irradiation time, from 3.5 to 60 min.

The photodynamic therapy sessions employ the remote technique of irradiation. The distance from the light guide fiber end-face to the object exposed varies from 0.2 to 2.5 cm depending on the design features of the radiation source.

With these devices, studies of a new class of photosensitizers absorbing in the long-wave region of the spectrum were facilitated, and their testing both on tumor cells of different geneses and on tumor-bearing animals was brought to a higher level. The existing facilities based on a halogen lamp with a set of filters were replaced by monochromatic LED light sources.

Improving the Efficacy of the Photodynamic Therapy Method

We developed methods combining photodynamic therapy with chemotherapy and with pulsed laser hyperthermia, as well as new techniques for low-intensity and pulsed laser photodynamic therapy treatment.

Low-Intensity Irradiation Regimes in Photodynamic Therapy

Currently, the photodynamic therapy treatment sessions in the clinic employ laser radiation of the conventional power ($50\text{--}100 \text{ mW cm}^{-2}$ and above). However, for some tumor localizations this irradiation regime is unacceptable because of a high risk of severe side reactions. This problem can be overcome by using low irradiation doses and low radiation power densities.

The experiments with Photosens in which a low-intensity photochemical action was produced on the tumor cells *in vitro* (cell culture HEP2) showed that the most efficacious regime is that combining the optical radiation power density P_s of 10 mW cm^{-2} and the energy density P_w of 3 J cm^{-2} ($\text{IC}_{90} 2.6 \pm 0.7 \mu\text{M}$). An increase in the power density to 20, 40, and 80 mW cm^{-2} (at the radiation energy density of 3 J cm^{-2}) causes the treatment efficacy to decrease by half ($\text{IC}_{90} 5.9 \pm 0.4 \mu\text{M}$).

Table 11. Antitumor efficacy and tolerability of photodynamic therapy with Photosens in relation to irradiation parameters. Experimental animals: mice with sarcoma S37. P_s is the radiation power density, and P_w , radiation energy density^a

Dose, mg kg ⁻¹	Irradiation pa- rameters		Death of mice from phototoxic shock, %	Severity of local-tissue reaction	Complete resorption of tumor lesion, %	Tumor growth inhibition, %			
	P_s , mW cm ⁻²	P_w , J cm ⁻²				observation time, days			
						6–7	8–9	10–12	14–15
5.0	100	90	0	++	0	54 ^b	51	23	9
5.0	25	90	0	++	0	72 ^b	76 ^b	77 ^b	78 ^b
5.0	12	90	66	+++	34	100 ^b	100 ^a	100 ^b	100 ^b
5.0	12	45	0	+++	100	100 ^b	100 ^b	100 ^b	100 ^b
2.5	12	45	0	++	0	100 ^b	98 ^b	95 ^b	74 ^b
1.25	12	45	0	++	0	84 ^b	87 ^b	82 ^b	74 ^b
0.6	12	45	0	+	0	44	51	47	54 ^b

^a (+) Mild, (++) moderately expressed, and (+++) severe reaction. ^b The tumor lesion volumes for the experimental and control groups of animals were significantly different ($p < 0.05$).

Photodynamic therapy in the conventional irradiation regime (100 mW cm⁻², 90 J cm⁻²) using Photosens at the therapeutic dose of 5 mg kg⁻¹ led to inhibition of the growth of S37 sarcoma by 54–51% within 8 days (Table 11). Reduction of the power density to 12 mW cm⁻² at the same radiation energy densities and photosensitizer dose causes a significant increase in the treatment efficacy: The maximum therapeutic effect (complete resorption of the tumor lesion) was observed in 34% of the mice. However, at high P_w (90 J cm⁻²) with a decrease in P_s an increase in the treatment efficacy was paralleled by that in the general toxicity, which led to the death of the experimental animals from phototoxic shock and to prominent local tissue reactions in the irradiated area.

The option chosen for optimizing the “low-intensity” irradiation regime consisted in reduction of both the light dose and the photosensitizer dose.

The optimal light exposure parameters in photodynamic therapy with Photosens, providing the maximum therapeutic effect, are as follows: radiation power density 10 mW cm⁻² and light dose 30 J cm⁻² (TGI 100–97%) and 40 J cm⁻² (complete resorption of the tumor lesion).

A decrease in the Photosens dose from 5 to 0.6 mg kg⁻¹ caused the treatment efficacy to decrease. The differences in the degree of antitumor effect from photodynamic therapy with Photosens in the “low-intensity” and conventional irradiation regimes may be

due to different rates of oxygen utilization in the irradiated area. In studies of the local-irritant action of photodynamic therapy with Photosens and Alasens-lio in the pleural and peritoneal cavities, safe “low-intensity” irradiation regimes [28] were identified.

Based on the data obtained, a clinical study protocol was developed for intraoperative photodynamic therapy in the “low-intensity” exposure regimes useful for treatment of patients with lung, stomach, and colon cancer.

Pulsed Laser Photodynamic Therapy

The VELIT Research and Production Enterprise, Limited Liability Company (Istra, Moscow oblast), developed KULON-MED multifunctional laser medical device for scientific and practical medical applications. The device generates laser radiation (coherent, monochromatic, collimated) in the visible, green, yellow, red, and near-IR spectral regions in the pulsed laser operation mode. One of the applications of the device is photodynamic therapy of malignant tumors of the major locations and non-neoplastic diseases [29].

We examined the antitumor efficacy of photodynamic therapy using light dose fractionation on mice inoculated subcutaneously with S37 sarcoma to the outer surface of the femur. The radiation sources were a KULON-MED 03 setup operated in the pulsed irradiation regime and a BIOSPEK laser operated in

Table 12. Antitumor efficacy of combined use of the photodynamic therapy (PDT) with Photosens and chemotherapy with 5-fluorouracil (5-FU). Experimental animals: mice with P388 leucosis

Treatment scheme	Efficacy	Tumor growth inhibition, %				Life span, %			Sum of effects	K^a
		observation time, days				PDT + 5-FU	PDT	5-FU		
		8	10	13	15					
5-FU, PDT after 24 h	Relative to PDT	−10	41	29	2	15.1±5.7	4.5±2.1	7.5±0.7	12.0±0.7	1.23±0.32
	Relative to 5-FU	67	81	76	78					
5-FU, PDT after 2 h	Relative to PDT	70	70	54	54	15.0±3.6	6.0±3.0	7.3±3.5	13.3±5.8	1.18±0.22
	Relative to 5-FU	85	87	85	84					
PDT, 5-FU after 2 h	Relative to PDT	52	36	51	54	24	9	11	20	1.20
	Relative to 5-FU	81	72	84	84					
PDT, 5-FU after 24 h	Relative to PDT	59	55	50	67	26.3±5.5	6.0±3.0	8.3±2.9	14.3±4.2	1.91±0.62
	Relative to 5-FU	80	80	80	81					

^a The ratio of the effect from the combined treatment to the sum of the effects from individual PDT and 5-FU.

the continuous-wave irradiation mode (for comparison). Photosens was administered at the dose of 2 mg kg^{–1} 4 h prior to the radiation exposure. A higher efficacy of treatment with Photosens in the pulsed irradiation regimes was demonstrated. The most efficacious was the following regime: 1-s irradiation at the frequency of 14 kHz –1-s pause. Long-term (for over 21 days after treatment) tumor growth inhibition (88–100%) and a 61% life span were observed.

Based on the data obtained, a clinical study protocol for the pulsed irradiation mode in photo-dynamic therapy of cancer patients was developed.

Photodynamic Therapy Combined with Chemotherapy

In the case of large tumors, photodynamic therapy is less efficacious, particularly due to the difficulty in delivering the light with effective “therapeutic” intensity to all areas of the tumor, nonuniform saturation of the tumor focus with oxygen, and heterogeneous distribution of the photosensitizer therein. One way to improve the efficacy of photodynamic therapy is via combining with chemotherapy.

The combined treatment efficacy depends on the sequence and the interval between the chemotherapy and photodynamic therapy sessions [30, 31]. Considering the fact that, in treatment of skin tumors (skin metastases of breast cancer, melanoma, and multiple basal-cell carcinoma), resorption of neo-

plasms in the zone exposed to optical irradiation in a number of cases is accompanied by growth of tumor foci at other sites, it is reasonable to combine the local and systemic antitumor effects.

The antitumor efficacy of the photodynamic therapy combined with chemotherapy was determined for mice with P388 lymphocytic leukemia subcutaneously inoculated in the gastrocnemius muscle on the outer side. As photosensitizer served Photosens [32], which was administered at the dose of 5.0 mg kg^{–1} on day 5 of the tumor growth.

The radiation exposure of the primary lesion was performed on day 6 of the tumor growth against the background of a histologically verified widespread tumor process. Cytotoxic agents used for chemotherapy were 5-fluorouracil, adriamycin, cisplatin, and cyclophosphamide. The combined treatment was performed by different schemes: the cytostatics were administered intravenously as one therapeutic dose against the background of Photosens before and after the radiation exposure. Table 12 lists the results from exposure of the primary tumor focus to photodynamic therapy (PDT) in combination with 5-fluorouracil. Combinations with therapy using other cytotoxic agents proved to be successful as well.

Comparison of the results from application of different therapy regimes shows that treatment in the “PDT + cytostatic agent after 24 h” and “PDT + cytostatic agent after 2 h” regimes leads to significant

Table 13. Antitumor efficacy of photodynamic therapy (PDT) with Photosens, laser-induced hyperthermia (LIH), and their combination with respect to PC1 tumor

Treatment scheme	Presence of tumors up to 10 cm ³ in volume, %	Time of tumor volume increase to 10 cm ³ , day	Presence of tumors with doubled volume, %	Tumor volume doubling time, day	Tumor growth inhibition, %	Results of therapy		
						complete regression, %	recurrence, %	recurrence-free period, day
PDT→LIH (43°C/ 800 mW cm ⁻² / 30 min)	0	180	28.6	71.9±51.1	84.9	85.7	16.7	95±3
PDT+LIH (41°C/ 400 mW cm ⁻² / 30 min)	0	83–180	0	37.7±15.3	94.4%	100	42.8	59.7±16.0
LIH (43°C/ 800 mW cm ⁻² / 30 min)	100	12–75	100	19.0±8.9	24.6	16.7	100	8±2
LIH (41°C/ 400 mW cm ⁻² / 30 min)	100	18–40	100	16.1±6.4	23.3	0	–	–
PDT with Photosens (2 mg kg ⁻¹)	41.7	12–180	66.7	25.0±12.3	64.1	66.7	37.5	68±9.4
Photosens (2 mg kg ⁻¹)	100	13–27	100	3.2±0.4	3.3	0	–	–
Control	100	6–27	100	3.2±0.6	–	0	–	–

inhibition of the tumor growth (up to 76–91%) and to an increase in the life span of the mice (by 26–49%) compared to the untreated animals. Treatment with the cytostatic administered after photodynamic therapy treatment proved to be slightly more efficacious (as a trend) than in the case of chemotherapy prior to PDT [33–36].

Our data allowed the combined use of photodynamic therapy and chemotherapy with cytotoxic agents to be recommended for both radical and palliative treatment of cancer patients. The most promising scheme is that based on introduction of an anticancer drug 2–24 h after photodynamic therapy treatment. Based on these data, clinical study protocols were developed for photodynamic therapy combined with anticancer drug therapy of skin and gastric cancer with Photosens and cytostatic drugs 5-fluorouracil, adriamycin, cisplatin, and cyclophosphamide.

Photodynamic Therapy Combined with Pulsed Laser Hyperthermia

Hyperthermia treatment results in a larger thermal damage to tumors in comparison with normal tissues. Tumors are more poorly vascularized than are normal tissues, so they tend to concentrate the heat energy via reduced heat transfer capacity. Furthermore, hypoxic cells possess enhanced thermal sensitivity due to low pH and deficiency of nutrients. Thus, hyperthermia causes damage to hypoxic regions in tumors above all. By contrast, well-oxygenated tumors with a developed network of blood vessels are more sensitive to photodynamic therapy [37], which constitutes an additional argument in favor of the combined use of PDT with hyperthermia.

As known, warming the tumor tissue to 42–44°C causes cell destruction. At a temperature of 40–42°C, the injury is less pronounced, but the action of

anticancer drugs and ionizing radiation is potentiated. At 38–40°C, increased metabolism and growth of tumors take place [38]. It is also known that the intensity of necrobiotic changes (irreversible changes in cells) depends on the time of maintaining an elevated temperature in the tumor.

The method of combined use of laser-induced hyperthermia and photodynamic therapy was studied on outbred rats (males) with PC1 tumor subcutaneously inoculated on the side. Treatment was started upon reaching the tumor volume of $3.9 \pm 2.0 \text{ cm}^3$. The laser-induced hyperthermia regime was as follows: irradiation wavelength 1064 nm, setpoint temperature 41 or 43°C, setpoint temperature maintaining time 30 min, and radiation power density 800 or 400 mW cm^{-2} . The photodynamic therapy regime was as follows: one day after administration of 2 mg kg^{-1} Photosens, radiation power density 142 mW cm^{-2} , light dose 150 J cm^{-2} .

The combined treatment by photodynamic therapy and the laser-induced hyperthermia (LIH) was performed by the following schemes:

PDT→LIH (43°C/800 mW cm^{-2} /30 min),
LIH immediately after PDT, (1)

PDT+LIH (41°C/400 mW cm^{-2} /30 min),
LIH and PDT started simultaneously, (2)

PDT→LIH (41°C/400 mW cm^{-2} /30 min),
LIH immediately after PDT, (3)

LIH (41°C/400 mW cm^{-2} /30 min)
→ PDT immediately after LIH. (4)

The preliminary experiments showed that schemes (1) and (2) are the most efficacious (Table 13). According to our results, both direct and remote, the combined treatment of rat PC1 tumor by PDT→LIH (43°C/800 mW cm^{-2} /30 min) provided a more pronounced antitumor effect [39]. Combined use of the both methods at temperatures of 41 and 43°C for 30 min, both in a sequence and simultaneously, was satisfactorily tolerated by the animals and did not lead to their death from toxicity. No behavioral changes were detected throughout the period of observation of the animals.

Thus, combinations of photodynamic therapy with laser hyperthermia in the regimes tested are superior in efficacy to these methods when used alone and also are safe from toxicological viewpoint. Based on the data obtained, “A Prospective Open-Label Study of the Efficacy of Photosens for Combined Use of Laser Hyperthermia with Photodynamic Therapy” clinical

protocol was developed for treatment of patients with recurrent basal-cell skin cancer and intradermal and subcutaneous metastases of breast cancer.

CONCLUSIONS

Fifteen years of studies in the field of experimental photodynamic therapy have culminated in development of the “Methodological Recommendations for Study of Photoinduced Antitumor Properties of Drugs” [1], whereby highly efficacious photosensitizers, in particular, a new generation of photosensitizers absorbing in the long-wave region of the spectrum (metal-free tetra- and octacationic tetrahydroporphyrin derivatives) were identified. The photosensitizers tested were used for development of new original agents and their dosage forms Alasens-lio, Alasens-gel, Hexasens-lio, Phthalosens-lio, Holo-sens-lio, and Holosens-gel whose preclinical testing has been completed to date. Based on the results of clinical trials of Alasens-lio, a permission for its use in fluorescence diagnosis of a number of malignant neoplasms (bladder, mucosa of the mouth and digestive tract, larynx, trachea, bronchi) and in photodynamic therapy of superficial tumors of the skin (excluding melanoma) was obtained.

For experimental photodynamic therapy, new original techniques employing the “low-intensity” and pulsed irradiation regimes were devised, as well as techniques combining photodynamic therapy with conventional treatment methods (chemotherapy and laser hyperthermia). Based on these techniques, clinical trial protocols were developed, which allowed expanding the application scope for the photodynamic therapy method.

REFERENCES

1. Yakubovskaya, R.I., Kazachkina, N.I., Karmakova, T.A., et al., in *Rukovodstvo po provedeniyu doklinicheskikh issledovaniy lekarstvennykh sredstv* (Guidelines for Preclinical Trials of Drugs), Moscow: Grif i K, 2012, part 1, pp. 657–671.
2. Plyutinskaya, A.D., *Cand. Sci. (Biol.) Dissertation*, Moscow, 2012.
3. Feofanov, F., Grichin, A., Karmakova, T., Kazachkina, N., et al., *Photochem. Photobiol.*, 2002, vol. 75, no. 5, pp. 527–533.
4. Plyutinskaya, A.D., Yakubovskaya, R.I., Luk'yanets, E.A., et al., *Ros. Onkol. Zh.*, 2011, no. 2, pp. 25–27.
5. RF Patent no. 2476218.

6. RF Patent no. 2479585.
7. Denisova, E.D., Apolikhina, I.A., and Bulgakova, N.N., *Akush. Ginekol.*, 2011, no. 3, pp. 17–20.
8. Kovneristyi, A.E., Kolyadenko, V.G., Kolyadenko, E.V., et al., *Ukr. Zh. Dermatol., Venerol., Kosmetol.*, 2005, no. 4, pp. 6–10.
9. Novikova, E.G., Chulkova, O.V., Filonenko, E.V., et al., *Ros. Onkol. Zh.*, 2010, no. 2, pp. 25–28.
10. Chekhun, V.F., Gamaleya, N.F., and Kutsenok, V.V., *Onkologiya*, 2003, no. 3, pp. 239–243.
11. Yakubovskaya, R.I., Kazachkina, N.I., Plyutinskaya, A.D., et al., *Ros. Onkol. Zh.*, 2009, no. 2, pp. 17–23.
12. Sakharova, N.A., Osikov, N.V., Negrimovsky, V.M., et al., *Progress in Biomedical Optics and Imaging of SPIE Therapeutic Laser Applications and Laser–Tissue Interactions III: SPIE*, OSA–Optical Society of America, Munich, 2007.
13. Osikov, N.V., Kazachkina, N.I., Pankratov, A.A., et al., *Khim. Tekhnol.*, 2011, no. 6, pp. 378–383.
14. Kazachkina, N.I., Pankratov, A.A., Yakubovskaya, R.I., and Negrimovskii, V.M., *Ros. Bioterap. Zh.*, 2011, no. 2, vol. 10, pp. 67–71.
15. Pankratov, A.A., Venediktova, Yu.B., Andreeva, T.A., et al., *Ros. Onkol. Zh.*, 2010, no. 3, pp. 19–21.
16. Morozova, N.B., Yakubovskaya, R.I., Derkacheva, V.M., and Luk'yanets, E.A., *Ros. Onkol. Zh.*, 2007, no. 1, pp. 37–43.
17. Yakubovskaya, R.I., Morozova, N.B., Pankratov, A.A., et al., *Ros. Onkol. Zh.*, 2006, no. 3, pp. 26–32.
18. Pankratov, A.A., Andreeva, T.A., and Yakubovskaya, R.I., *Ros. Onkol. Zh.*, 2006, no. 6, pp. 31–34.
19. Morozova, N.B., Yakubovskaya, R.I., Chissov, V.I., et al., *Ros. Bioterap. Zh.*, 2007, no. 2, pp. 50–54.
20. Strakhovskaya, M.G., Kuz'min, S.G., and Zhukhovitskii, V.G., *Materialy VI nauchno-prakticheskoi konferentsii "Farmakologicheskie i fizicheskie metody lecheniya v otorinolaringologii"* (Proc. IV Scientific and Practical Conf. "Pharmacological and Physical Treatment Methods in Otorhinolaryngology," Russia, 2008.
21. Morozova, N.B., Yakubovskaya, R.I., Chissov, V.I., et al., *Ros. Onkol. Zh.*, 2012, no. 1, p. 23–28.
22. Osikov, N.V., Morozova, N.B., Yakubovskaya, R.I., et al., *Khim. Tekhnol.*, 2011, no. 8, pp. 501–507.
23. RF Patent no. 2465899.
24. Zharkova, N.N., *Cand. Sci. (Phys.–Math.) Dissertation*, Moscow, 1992.
25. Zharkova, N.N., Kozlov, D.N., Polivanov, Yu.N., and Pykhov, R.L., *Proc. SPIE*, 1994, vol. 2328, pp. 196–201.
26. *Rukovodstvo po eksperimental'nomu (doklinicheskomu) izucheniyu novykh farmakologicheskikh veshchestv* [Guidelines for Experimental (Preclinical) Trial of New Pharmacological Agents], Khabriev, R.U., Ed., Moscow: Meditsina, 2005.
27. Feofanov, A., Grichine, A., Kudelina, I., et al., *Rus. J. Bioorg. Chem.*, 1999, v. 25, no. 12, pp. 793–802.
28. Pankratov, A.A., Venediktova, Yu.B., Plyutinskaya, A.D., et al., *Ros. Onkol. Zh.*, 2008, no. 6, pp. 28–32.
29. Chissov, V.I., Sokolov, V.V., Yakubovskaya, R.I., et al., *Lazer. Med.*, 2011, vol. 15, no. 4, pp. 40–47.
30. Cowled, P.A., Mackenzie, L., and Forbes, I.J., *Cancer Res.*, 1987, vol. 47, no. 4, pp. 971–974.
31. Ma, L.W., Berg, K., Danielsen, H.E., et al., *Cancer Lett.*, 1996, vol. 109, nos. 1–2, pp. 129–139.
32. Luk'yanets, E.A., *Ros. Khim. Zh.*, 1998, vol. 42, no. 5, pp. 9–16.
33. Kazachkina, N.I., Morozova, N.B., Yakubovskaya, R.I., and Luk'yanets, E.A., *Ros. Onkol. Zh.*, 2006, no. 6, pp. 34–37.
34. Kazachkina, N.I., Morozova, N.B., and Yakubovskaya, R.I., *Ros. Onkol. Zh.*, 2009, no. 3, pp. 21–24.
35. Kazachkina, N.I., Yakubovskaya, R.I., and Morozova, N.B., *Ros. Onkol. Zh.*, 2011, no. 6, pp. 26–29.
36. Kazachkina, N.I., Yakubovskaya, R.I., Morozova, N.B., et al., *Proc. 6th Int. Congr. of the World Association of Laser Therapy*, Limassol (Cyprus), 2006, pp. 117–120.
37. Belous, T.A., Frank, G.A., Sokolov, V.V., and Aristarkhova, E.I., *Ros. Onkol. Zh.*, 1998, no. 1, pp. 15–18.
38. Kirsch, R. and Schmidt, D., *Zentralbl. Chir.*, 1966, Sept. 3, vol. 91, no. 36, pp. 1297–1312.
39. Kazachkina, N.I., Krylova, G.P., Sokolov, V.V., et al., *Proc. 6th Int. Congr. of the World Association of Laser Therapy*, Limassol (Cyprus), 2006, pp. 113–116.